ADVANCED OPTICAL MATERIALS
www.advopticalmat.de

Integration of Laser-Patterned Photonic Crystals in Si Solar Cells

Michael Rienäcker, Udo Römer, Jan Krügener, Jovan Maksimovic, Tomas Katkus, Dominyka Stonytė, Soon Hock Ng, Haoran Mu, Nguyen Hoai An Le, Zahra Khajehsaeidimahabadi, Gediminas Seniutinas, Justas Baltrukonis, Orestas Ulčinas, Mindaugas Mikutis, Vytautas Sabonis, Yoshiaki Nishijima, Sajeev John, Saulius Juodkazis, and Robby Peibst*

Photonic crystal (PhC) light trapping is predicted to enhance absorption beyond the Lambertian limit, potentially increasing silicon solar cell efficiencies above 28%. However, integrating PhC structures into high-efficiency devices at scale remains challenging. PhC textures are integrated into back-contacted silicon solar cells by combining femtosecond laser ablation of alumina masks with dry etching. Excellent surface passivation is maintained using an isotropic defect-removal process based on ammonia peroxide mixture (APM). This preserves the front-side texture and keeps optical reflection low. The PhC-patterned cells deliver minority carrier lifetimes and carrier collection efficiencies comparable to state-of-the-art high efficiency devices. A certified efficiency of 23.1% is achieved. The quantum efficiency of the thick (190–290 µm) solar cells, however, shows no clear wave-optical resonances under standard conditions, despite the high structural and electronic quality. Scalability is improved by applying direct laser writing with Gaussian and Bessel beams and developing a periodically anchored mask design. This enables uniform, large-area patterning. These advancements mark a key step toward the practical implementation of PhC-enhanced silicon photovoltaics.

1. Introduction

As silicon solar cells become thinner to reduce material consumption, CO_2 footprint and energy payback time, increasingly effective light trapping is required to maintain and improve conversion efficiency. Achieving light trapping close to the Lambertian limit or beyond it, would enable efficiencies exceeding 28%,[1] approaching the fundamental Shockley–Queisser limit of 33% for Si under one-sun illumination. The current world record efficiency of 27.8% for large-area (133.6 cm^2) n-type silicon interdigitated back-contact (IBC) cells[2] already demonstrates impressive progress but still leaves headroom for improvement. Photonic crystal (PhC) structures have emerged as a promising light trapping approach, capable of enhancing optical absorption beyond the classical ray optics limit by exploiting wave-interference effects.[3–5] Experimental demonstrations on thin

M. Rienäcker, U. Römer, R. Peibst
Institute for Solar Energy Research in Hamelin (ISFH)
Am Ohrberg 1, 31860 Emmerthal, Germany
E-mail: rienaecker@isfh.de
J. Krügener, R. Peibst
Institute of Electronic Materials and Devices
Leibniz Universität Hannover
Schneiderberg 32, 30167 Hannover, Germany

J. Maksimovic, T. Katkus, D. Stonytė, S. H. Ng, H. Mu, N. H. A. Le, Z. Khajehsaeidimahabadi, G. Seniutinas, S. Juodkazis
Optical Sciences Centre
ARC Training Centre in Surface Engineering for Advanced Materials (SEAM)
Swinburne University of Technology
Hawthorn, Victoria 3122, Australia
D. Stonytė, S. Juodkazis
Laser Research Center
Physics Faculty
Vilnius University
Saulėtekio Ave. 10, Vilnius 10223, Lithuania
J. Baltrukonis, O. Ulčinas, M. Mikutis, V. Sabonis
Altechna R&D
Workshop of Photonics
Mokslininkų str. 6A, Vilnius 08412, Lithuania

The ORCID identification number(s) for the author(s) of this article can be found under https://doi.org/10.1002/adom.202501781

DOI: 10.1002/adom.202501781

silicon-on-insulator (SOI) layers structured by electron beam lithography (EBL)[4] have shown substantial enhancement in absorption near the absorption edge. More recently, theoretical studies have predicted that PhC light trapping could also benefit intermediate-thickness Si solar cells,[6] provided that coherent interference is preserved within the device. Although the optical advantages of PhC light trapping have been demonstrated, the integration of such structures into fully functional silicon solar cells has yet been only realized on a moderate efficiency level of up to around 16% using SIO wafer and photo-lithographic pattering.[7,8] At the same time, the actual benefit of PhC light trapping in realistic high-efficiency Si solar cells remains under discussion. While strong absorption enhancements have been demonstrated in thin, idealized structures, it is still debated whether coherent interference effects persist in intermediate-thickness devices under practical operating conditions.[9,10] In this context, there is a clear need for experimental benchmarks on advanced device platforms that can either verify or challenge these predictions. Our work provides such a data point: we integrate PhC textures into POLO^2-IBC solar cells, a state-of-the-art architecture with efficiencies exceeding 26%, thereby enabling an assessment of PhC concepts under realistic, high-performance conditions. A major challenge for practical implementation is the development of scalable fabrication methods. Traditional approaches such as electron beam lithography or photolithography are unsuitable for high-volume manufacturing because of their low throughput and high costs. In contrast, laser-based processing is already widely employed in the photovoltaic industry, particularly for rear-side structuring, and offers a promising pathway for large-area PhC fabrication.[11–14] In this work, we integrate laser-patterned PhC textures into high-efficiency silicon solar cells using femtosecond (fs) laser ablation of alumina masks, initially employing Gaussian beams. To overcome limitations related to surface topography and patterning area, we implement Bessel beam-based laser writing and a periodically anchored mask design that improves stability during plasma etching.[15] The patterned alumina masks are transferred into the silicon surface via dry plasma etching, which may be replaced by scalable alternatives such as atmospheric pressure dry etching.[16] To restore high-quality surface passivation after plasma processing, we develop an isotropic defect-removal step based on ammonia peroxide mixture (APM) etching. This enables carrier lifetimes comparable to those of high-efficiency POLO^2-IBC cells, which feature polycrystalline silicon on oxide (POLO) passivating contacts in an interdigitated back-contact architecture. These cells provide a robust platform for assessing photonic crystal (PhC)-induced light trapping enhancements. We begin our analysis with this POLO^2-IBC reference cell, employing conventional random pyramid (RP) front-side texturing. It serves as a performance baseline for evaluating the impact of integrated PhC textures presented in the following sections.

2. POLO^2-IBC Reference Cell with Random Pyramid Texturing

The reference POLO^2-IBC solar cells are fabricated at ISFH using 300 µm-thick p-type FZ silicon wafers (~1.3 Ω ·cm) and a process previously described in detail.[17,18] The cell features a rear-side interdigitated POLO junction structure and a random pyramid (RP) front-side texture formed by alkaline wet etching. Both front and rear surfaces are passivated with a multi-layer dielectric stack ($AlO_x/SiN_y/SiO_z$). A schematic cross-section after front-end processing is shown in **Figure 1a**.

Figure 1c shows the minority carrier lifetime map of the POLO^2-IBC cell precursor with random pyramids after front-end processing. The effective lifetime for the cell precursor with random pyramids at 0.25 suns illumination reaches 2.4 ms within the cell areas. The implied current–voltage (I–V) characteristic deduced from illumination intensity dependent lifetime measurements yields an implied pseudo-efficiency of up to 26.7% and demonstrates the high potential of our baseline cells at this stage of processing. During the back-end processing, rear-side metallization is performed by local laser contact opening of dielectric layers and Al evaporation, followed by contact separation via laser ablation and wet etching. The baseline POLO^2-IBC cell yields an independently confirmed (ISFH CalTeC) efficiency of 26.02% with an open-circuit voltage V_{OC} of 730.2 mV, a short-circuit current density J_{SC} of 42.2 mA/cm^2 and a fill factor FF of 84.44%. The electrical collection efficiency derived from the internal quantum efficiency (IQE) for the wavelengths between 700 and 900 nm equals 98.5% and underlines the excellent recombination behavior, especially the excellent surface passivation of the baseline cell. The recombination pre-factor $J_{01} \approx 18$ fA/cm^2 from the current-voltage characteristic limiting the V_{OC} is composed of ~4–5 fA/cm^2 for the front side passivation, ~1–2 fA/cm^2 for the rear side passivation and ~5–10 fA/cm^2 for the recombination within the wafer. Thus, reducing J_{01} requires enhanced front-side passivation and thinner wafers. However, 300 µm is currently required to achieve the high J_{SC} with the current light trapping scheme using random pyramids. Improved light trapping allows for a reduction in absorber thickness without compromising the J_{SC}.

3. POLO^2-IBC Cell with Photonic Crystal Light Trapping by Gaussian Beam Pattering

The PhC-patterned POLO^2-IBC cells are fabricated using the same baseline process described above, with the key modification of introducing a photonic crystal texture on the front side. This texture is defined by femtosecond laser ablation of an alumina mask using a Gaussian beam (515 nm), followed by dry reactive ion etching (RIE) of the silicon surface. The PhC regions are patterned in localized 2 × 2 cm^2 areas on the wafer for experimental evaluation. Figure 1e shows an scanning electron microscope

Y. Nishijima
Department of Electrical and Computer Engineering
Graduate School of Engineering
Yokohama National University
79-5 Tokiwadai, Hodogaya-ku, Yokohama 240-8501, Japan
S. John
Department of Physics
University of Toronto
60 St. George Street, Toronto ON M5S 1A7, Canada
S. Juodkazis
WRH Program International Research Frontiers Initiative (IRFI)
Tokyo Institute of Technology
Nagatsuta-cho, Midori-ku, Yokohama, Kanagawa 226-8503, Japan

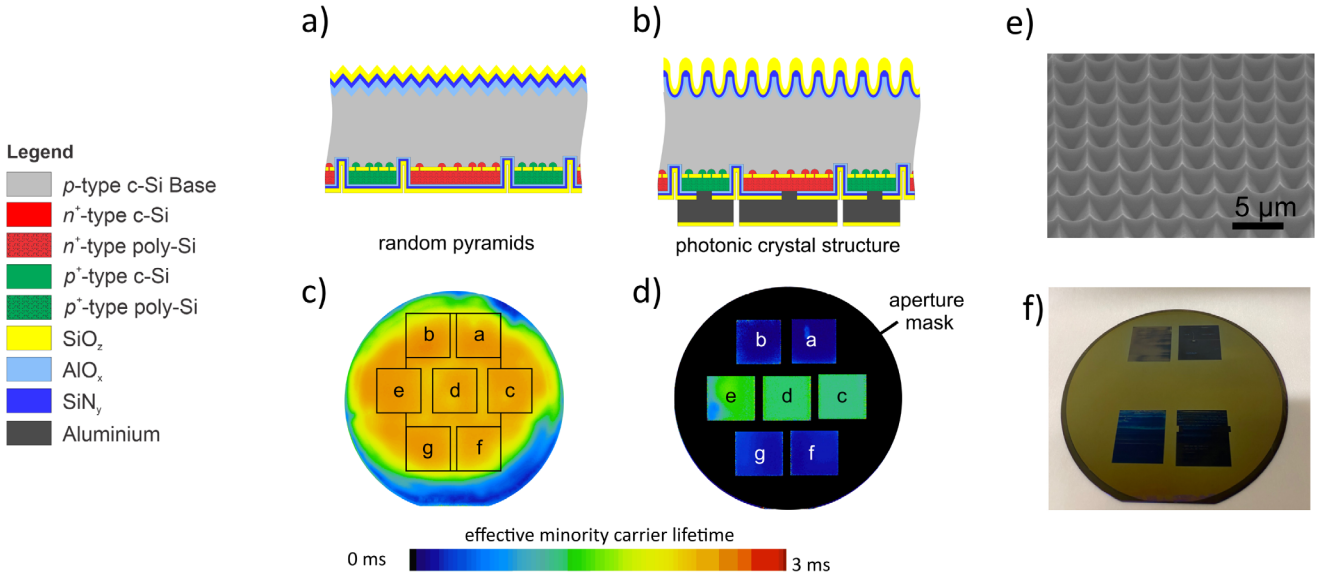

Figure 1. a,b) Schematic cross-section of the POLO^2-IBC cell precursor with random pyramids after passivation (a) and the finished POLO^2-IBC cell with a photonic crystal structure (b). c,d) Spatially resolved carrier lifetime of the cell structures shown in (a,b) at ~0.25 suns measured by the ILM method without (c) and with (d) aperture mask. The active cell areas of the seven solar cells are marked with squares a–g. e) SEM image of the photonic crystal structure with $\Lambda = 3.1$ µm period and f) photograph of the front side of the 4-inch cell wafer shown in (d) with four 2 × 2 cm^2 patterned cells.

(SEM) image of the PhC texture with a lattice constant of 3.1 µm. The cell wafer of the first POLO^2-IBC cell with photonic crystals after back-end processing is shown in Figure 1f and contains four 2 × 2 cm^2 structured regions (cells a, b, f, g in 1d) and three polished regions (cells c, d, e in Figure 1d). The non-patterned, polished cells in Figure 1d demonstrate high effective carrier lifetimes of up to 1.3 ms at 0.25 suns, while the patterned cells with photonic crystals show lower lifetimes of 100–200 µs. Note that the measurement in Figure 1d was performed for the finished cell and with an aperture mask to avoid charge carrier injection from the high lifetime perimeter region into the low lifetime region of cell (a,b,f,g). The latter effect otherwise leads to a large overestimation of the cell performance. The analysis of the lifetime vs. excess carrier density according to Kane & Swanson[19] reveals a surface recombination pre-factor (both sides) of approx. 6 fA/cm^2 for the non-patterned cells in Figure 1d. This indicates that the rear side of the cells is properly passivated. Thus, we concluded that the front side of the patterned cells still contains remaining defects and/or any contamination from the patterning process e.g. from RIE etching as reported elsewhere.[20] As a result, a low efficiency $\eta = 14.75\%$ was obtained from current–voltage measurements for our first solar cells with photonic crystals. The defects and any possible contamination at the front surface can be removed by wet chemically etching the Si surface before passivating it. However, we used cleaning sequences without any Si removal in this first attempt in order to maintain the optical properties of the photonic crystal structure. The application of an appropriate "gentle" etching step is investigated on the above described low-performing cell in the following. The gentle etching step is challenging because it requires the removal of defective Si from the surface while preserving the morphology of the photonic crystal structure. To achieve this, we used an isotropic ammonia peroxide mixture (APM) with a low etch rate of ~1–2 nm/min to enable highly controlled and iterative silicon removal. The inset of **Figure** 2a as shown in the current-voltage characteristic depicts schematically the expected mechanism of defect removal in APM after several iterations of etching.

Experimentally, we first remove all dielectric passivation layers from the low-performing cell in hydroflouric acid (HF). Then we perform the etching in APM for 75 min and passivate front and back with AlO_x for characterization of the lifetime and reflection properties. This process of etching, passivation, and characterization is repeated multiple times on the same cell. Figure 2a shows an improving lifetime from 350 µs before etching to 2.3 ms after 300 min. The latter is on a similar level as for the POLO^2-IBC cell with random pyramids in Figure 1c. Therefore, we conclude that removing between 300 and 600 nm of Si from the front surface (corresponds to 300 min of etching), yields a mostly defect-free front surface. On the other hand, Figure 2b shows a slightly increasing AM1.5G-weighted average front side reflection from 11.2% to 13.1% of the same sample from 75 min to 300 min of etching. We speculate that this increasing reflection results from the rounding of the PhC texture especially at the ridges in-between and on the facets of the inverted pyramids. The SEM image in the inset of Figure 2a confirms that the morphology of the photonic crystal structure is fully preserved after the APM etching, while the defects are effectively removed. However, this comes at the cost of a slight increase in front-side reflection. Based on these promising results, we apply the APM etching method to a second POLO^2-IBC cell wafer directly after the fabrication of the photonic crystal structure. The first POLO^2-IBC cell with PhC structure and the applied defect etch demonstrates a certified efficiency of $\eta = 23.1\%$ as shown in the current-voltage characteristic in **Figure** 3a. In addition to the PhC-patterned regions, the same wafer also contained an unpatterned planar reference cell at the center of the wafer without any front-side

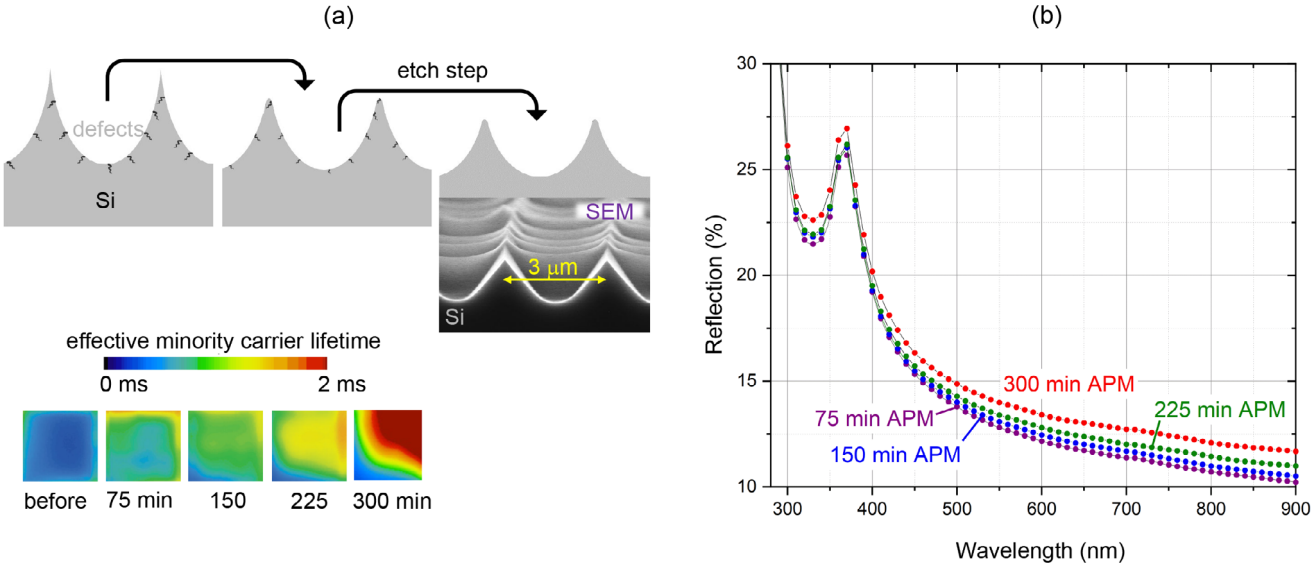

Figure 2. Passivation of PhC light trapping surface of the Polysilicon on Oxide Interdigitated Back Contacted - POLO^2-IBC cell. a) An isotropic defect removal etch process of the plasma-etched PhC texture by ammonia peroxide mixture (APM): time evolution of the lifetime of the same 2 × 2 cm^2 patterned area. Top-inset shows schematic changes of the PhC pattern and the SEM image after etching for 300 min. b) Reflectance spectra of the PhC texture after isotropic etching in APM measured on the same patterned area as in (a). Note: The samples were measured with an AlO_x passivation layer, thus without an effective antireflexion coating.

texturing. This reference cell confirms the excellent electronic quality of the POLO^2-IBC architecture, yielding a V_{OC} = 720.5 mV and a FF = 81.0%. However, as expected due to the absence of any front-side light trapping, the short-circuit current density was strongly reduced (J_{SC} = 36.2 mA/cm^2, η = 21.1%). In direct comparison, the PhC-patterned POLO^2-IBC cell after APM defect removal achieves a higher J_{SC} (39.5 mA/cm^2) and efficiency (23.1%) than this planar reference, confirming the optical benefit of the photonic crystal structures. At the same time, the performance remains below that of our optimized random-pyramid POLO^2-IBC baseline cells (J_{SC} = 42.2 mA/cm^2, η = 26.0%), which therefore continue to serve as the realistic benchmark for light-trapping performance. Figure 3b shows the external/internal quantum efficiency and the reflection of the first POLO^2-IBC cell with photonic crystals. We deduce a collection efficiency from the internal quantum efficiency (IQE) between 700 and 900 nm of 94.5%, which is on an high level, but slightly lower than for our POLO^2-IBC with random pyramids. The reflection properties reveal a slightly higher AM1.5G-weigthed average front side reflection of 3.9% as compared to 3.1% for the POLO^2-IBC cell with random pyramids. In the 1000 nm to 1200 nm range, we do not observe wave-interference-based optical resonances as reported for thinner structures.[4] In our intermediate wafer thickness of 190–290 µm, such features may be diminished by residual surface imperfections, parasitic absorption, or diffuse scattering in the bulk, as also reflected in the current debate on the limits of interference-based light trapping.[9,10] At the same time, the applied defect-removal etch enables the fabrication of a high-efficiency POLO^2-IBC cell with integrated photonic crystals. The resulting independently certified efficiency of 23.1% is the highest reported for a

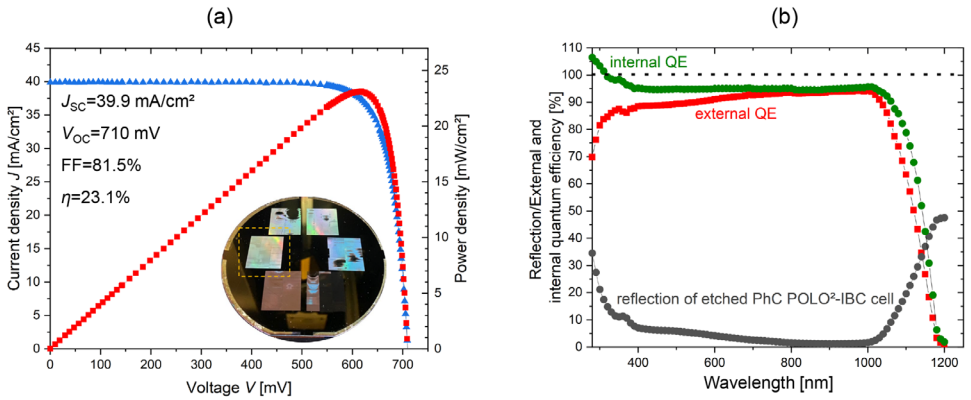

Figure 3. a) Current density–voltage (blue, left axis) and power density-voltage (red, right axis) characteristic of POLO^2-IBC cell with PhC light trapping after APM passivation (see Figure 2). Inset shows the wafer and selected cell. b) Spectra of reflectance, internal and external quantum efficiency (IQE & EQE).

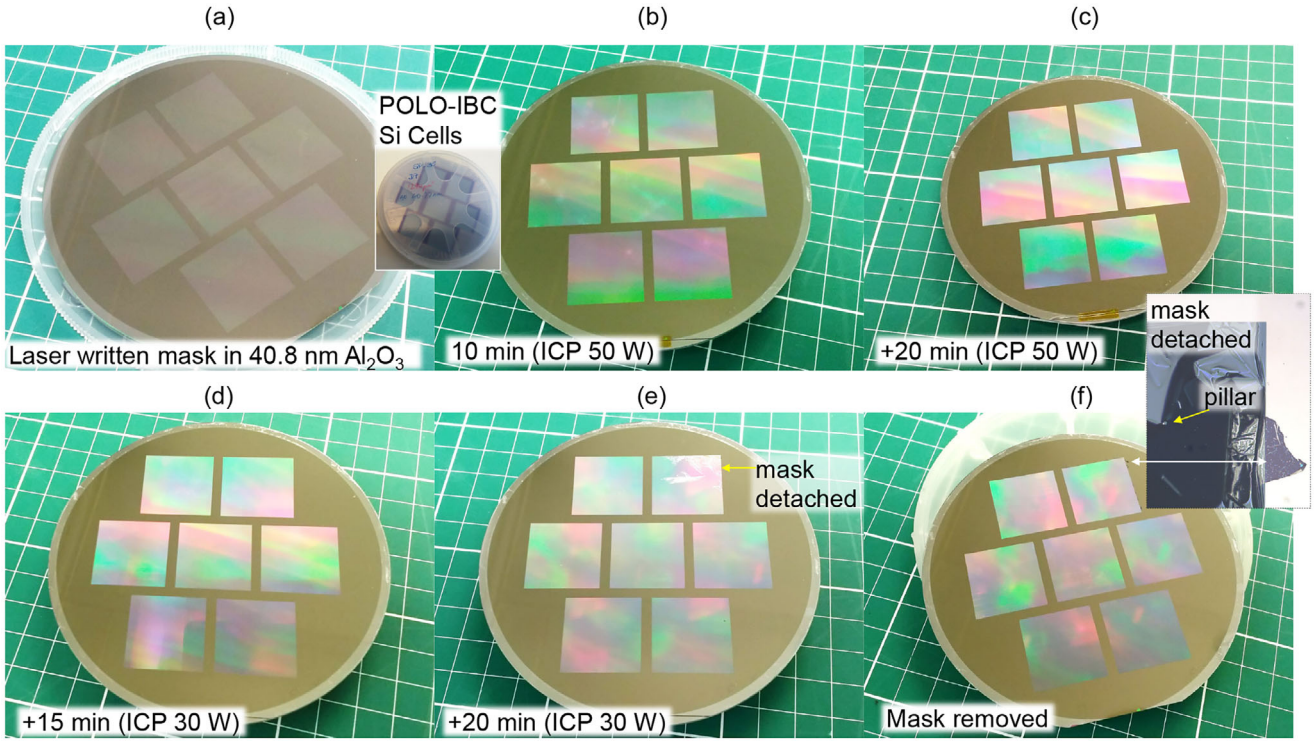

Figure 4. Front side of Si wafer with POLO^2-IBC solar cells (inset) at different processing steps: after fs-laser Bessel beam mask patterning (a), after different etching times at 50 W (b,c) and additional etch steps at 30 W (d,e), and after final mask removal by ultrasonic wash for 5 min in IPA bath (f).

solar cell featuring a photonic crystal texture and provides a robust benchmark for further development.

4. Advancing PhC Patterning

4.1. Bessel Beam Direct Laser Writing

Although the first demonstrator cells were manufactured using direct laser writing (DLW) with a Gaussian beam, the resulting structures exhibit certain inhomogeneities and defects, as shown in Figures 1f and 3a. These irregularities degrade the periodicity of the photonic crystal, potentially suppressing the intended light-trapping effects. Additionally, they contribute to an increased front-side reflection, further reducing the optical performance of the cell. A promising alternative is the use of Bessel beam DLW, which enables more uniform and high-precision patterning due to its self-reconstructing nature and extended depth of focus. Unlike Gaussian beams, which are highly sensitive to height variations of the surface, Bessel beams maintain consistent ablation over a larger focal distance. This makes them particularly suitable for structuring the etch masks on complete POLO^2-IBC cell wafers with height variations. The use of Bessel beams for mask patterning on solar cells has demonstrated improved uniformity across large areas, ensuring a more controlled transfer of the PhC texture into the silicon surface and reducing unwanted reflection losses (see details in Supporting Information).

Before implementing Bessel beam patterning in solar cell fabrication, we optimized the plasma etching protocol using only SF_6 gas to improve surface quality and minimize mesa widths between the PhC structures. **Figure 4** shows the inspection of a 290-µm-thick Si wafer with POLO^2-IBC solar cells at various stages of the etching process.

An ICP power of 50 W was used to achieve fast and uniform pattern transfer across the entire wafer. However, at the end of the process, etching at 30 W was applied to slow down the etch rate. This was particularly useful to safely approach the undercut condition, where the alumina mask begins to detach from the corner supports of the inverted pyramids (see Figure 4e). At this point, plasma etching was stopped, and the remaining alumina mask was removed in an ultrasonic isopropanol (IPA) bath, completing the pattern transfer into the silicon. Finally, we applied the Bessel beam DLW in combination with the optimized plasma etching protocol to fabricate 190-µm-thick POLO^2-IBC solar cells. After APM defect-removal etching and completion of the cell process as described above, the devices exhibited low recombination losses, with measured minority carrier lifetimes of $\tau_m \approx 2$–3 ms and open-circuit voltages $V_{OC} \approx 720$ mV. However, the short-circuit current density remained limited to $J_{SC} = 39.5$ mA/cm^2, which we attribute to increased front-side reflection, particularly in the short-wavelength range. This reflection is likely caused by planar valley regions within the inverted pyramids. These results confirm the compatibility of Bessel beam laser patterning and our optimized etching protocol with high-efficiency POLO^2-IBC solar cells. However, the expected increase in short-circuit current density due to enhanced light trapping from the PhC structure was not observed. We attribute this to residual optical losses from the planar valley regions and the thick wafers used herein. In future work, we will combine further improved PhC patterning

with thinner absorber wafers to maximize waver-interference effects and explore the full potential of wave-optical light trapping.

4.2. Periodically Anchored PhC Mask

Another major challenge in the fabrication of PhC structures is the intended underetch of the Al_2O_3 mask during reactive ion etching (RIE). As the etching progresses, the mask loses adhesion and eventually detaches from the silicon surface, leading to incomplete or distorted PhC patterns. To overcome this limitation, a periodically anchored PhC mask approach was developed. This method replaces continuous unstructured rows — which were previously required for mask adhesion — with periodically arranged nonablated support sites embedded in the PhC lattice. These local anchors stabilize the mask during plasma etching, enabling large-area patterning with consistent structure transfer and minimal defects (see details in Supporting Information). For the experimental implementation, we used p-type Si wafers and defined the pattern with a period of $\Lambda = 3.1$ µm. One out of every four sites was intentionally left unablated. As shown in our previous simulations,[15] this design performs almost identically in terms of light trapping compared to fully ablated patterns, while providing improved mechanical stability of the etch mask. The mask ablation was performed using 343 nm, 200 fs laser pulses focused through a $NA = 0.44$ objective lens, resulting in a focal spot diameter of approximately 0.95 µm on a 54-nm-thick alumina mask. Patterning was performed at a scan speed of 5 cm/s with a 0.1 MHz repetition rate. A bitmap-based scanning mode was used instead of the conventional shot-on-demand approach. This method significantly reduced positional errors that typically occur at high scan speeds and small pulse-to-pulse spacing.

We tested the process at various sample orientations, including $\theta = 0°$ relative to the Si [010] crystal direction, to evaluate potential anisotropy in the plasma etch step. However, the final texture formation was found to be governed by the PhC mask pattern itself rather than by the crystallographic orientation of the Si substrate.

Figure 5 summarizes the resulting PhC structures. The plasma etching was carried out using low-bias and high-ICP power conditions with SF_6, resulting in isotropic etching and uniform transfer of the pattern into the Si. The design of nonablated support pillars allows reliable mask adhesion throughout the etch process and enables seamless fabrication over large areas. Notably, the PhC features were observed to be nearly twice as deep compared to standard square-lattice structures without support sites. This increased depth may contribute to reduced front-side reflectance after APM treatment. Although the periodically anchored PhC mask patterning has not yet been applied to solar cells, it provides a reliable and well-controlled method for studying the impact of highly regular and defect-minimized photonic crystal structures in future cell architectures.

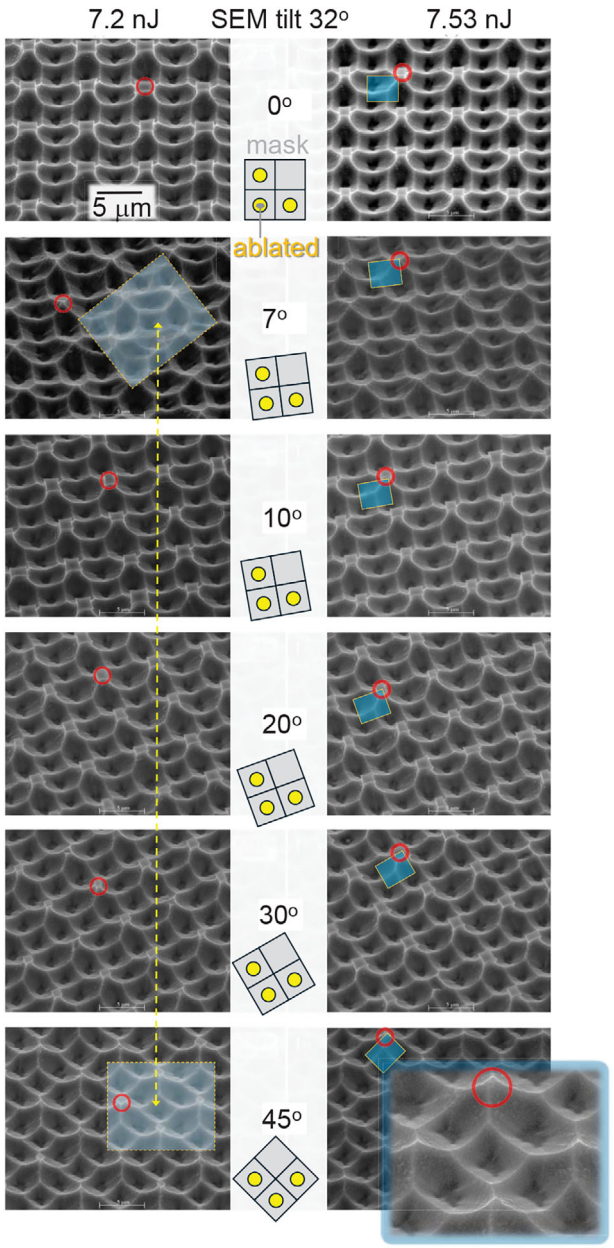

Figure 5. Periodically anchored PhC mask. SEM images of photonic crystal (PhC) structures etched into a Si wafer. A 50 nm-thick alumina mask with $\Lambda = 3.1$ µm period was patterned by 343 nm/200 fs laser pulses at $E_p = 7.2$ and 7.53 nJ, ablating three out of four sites per unit cell. The nonablated sites (marked by red circles in the SEM image) act as anchor points that mechanically stabilize the mask during plasma etching. The blue rectangles highlight the unit cells, which correspond to the schematic shown in the center. Plasma etching was performed for 35 min with SF_6:CHF_3:O_2 (10:2:2) at an ICP power of 180 W and a bias power of 5 W. The schematic (center) illustrates the periodic ablation pattern, rotated by 7°, 10°, 20°, 30°, and 45° relative to the Si(001) orientation. Orientation markers confirm that the etched profiles follow the mask pattern rather than the crystallographic direction. The inset shows a close-up of mesa-free PhC structures achieved with this approach.

5. Conclusion and Outlook

We demonstrated a Si solar cell with integrated photonic crystal (PhC) structures on the front-side, achieving an

independently certified efficiency of 23.1%. The PhC pattern was realized by fs-laser ablation of an alumina etch mask, initially using Gaussian beams and subsequently refined using Bessel beam direct laser writing (DLW). Bessel beam-based patterning significantly simplifies the fabrication process compared to conventional lithography by eliminating the need for resist coating, development, and lift-off steps. The use of a self-reconstructing Bessel beam enabled homogeneous mask patterning with sub-diffraction-limited hole sizes (400–600 nm) over cm^2-scale areas, even across non-flat surface regions affected by prior KOH etching. Combined with an optimized defect-removal etch of RIE-induced defects, this approach yielded textured surfaces with excellent carrier lifetimes ($\tau_m \approx$ 3 ms). Despite the successful integration of highly regular and electrically passivated PhC structures, we do not observe wave-interference-based optical resonances and no enhancement in short-circuit current density (J_{SC}) compared to conventional textures. This indicates that the simulated light-trapping benefits of PhC structures could not yet be realized experimentally in thick (190–290 µm) Si solar cells, highlighting the need for further investigation.

6. Methods and Materials

6.1. Fabrication of POLO⁴-IBC Solar Cells

6.1.1. Baseline Random Pyramid POLO²-IBC cell

The following baseline fabrication process yields our random pyramid (RP-)POLO²-IBC cell in Figure 1a and serves as the benchmark. We use 300-µm-thick 1.3 Ω cm, p-type FZ wafers and follow the process described elsewhere[17,18] to form the p^+-(i)-n^+ POLO interdigitated rear side by using amorphous Si, masked ion implantation and a subsequent wet oxidation and higher temperature process at 1035°C. Since the p^+-(i)-n^+ POLO rear side prevented us from implementing an advanced hydrogenation scheme for our POLO junctions,[18] we remove the p^+-(i)-n^+ junction by KOH etching through the lithographically patterned rear SiO_2 layer. This patterning step results in a trench separation between the *p*POLO und *n*POLO interdigitated regions and strips the SiO_2 and n^+ poly-Si layers from the front side. The latter results in a KOH-etch rough surface at the front side. In the next step, we strip the rear SiO_2 and create the random pyramid light trapping structure on the front side by an alkaline wet etch in a KOH-based texturing solution. We protect the rear side from texturing by using a PTFE sample holder. The front side receives a passivating anti-reflecting $AlO_x/SiN_y/SiO_z$ layer stack after a final RCA cleaning. We deposit a triple-layer stack of $AlO_x/SiN_y/SiO_z$ on the rear side, to passivate the trench region, to hydrogenate the POLO junctions and to facilitate the laser contact opening process.[21] Figure 1a schematically shows the cross-section of the cell precursor in this stage – after front-end processing. During the back-end processing, we locally laser open the rear side dielectric layers to form a contact with the evaporate Al electrode. After contact opening, we deposit a 10 µm-thick Al layer and a SiO_z layer on the rear side and perform the contact separation by locally laser ablating the SiO_z layer and etching the Al layer in the ablated region.

6.1.2. Modification of the Baseline Process for POLO²-IBC Cells with Photonic Crystal Structure

The fabrication of a photonic crystal structure on the KOH-etched, rough front side of the POLO²-IBC cell precursor wafer - as it would result from our optimized baseline fabrication process[17,18] - is challenging so far. Therefore, we adapt the baseline cell process, such that it leaves the chemically-mechanically polished (CMP) surface of the 280-µm-thick, 2.6 Ω cm, p-type FZ wafer intact throughout the cell process. For this purpose, we grow a protective 700-nm-thick SiO_2 layer prior to the cell process and laser ablate it from the rear side followed by a subsequent short KOH damage etch removal and a phosphorus diffusion gettering process. All subsequent steps follow the baseline process until the trench separation and poly-Si removal from the front side are carrier out. At this stage, we removed the thick protective SiO_2 layer from the polished front side of the cell precursors and fabricate the photonic crystal structure at the Swinburne University of Technology. The photonic crystal structures were fabricated with a novel direct laser write approach[11] as below with a subsequent reactive ion etching step. The reactive ion etching typically causes surface defects due to ion bombardment and implantation of contaminants with penetration from nanometers to a micrometer.[22,23] We used near-zero-bias plasma etch in order to reduce directional bombardment of Si surface by ions. Furthermore, such surface defects can be removed via wet processing in KOH or HNO_3:HF .[24,25] We apply an isotropic etching in an ammonia peroxide mixture (APM) with an etch rate of ~1 nm/min after dry plasma etch to remove the remaining surface defects ensuring an excellent passivation of the PhC light trapping surface, while maintaining the surface morphology almost unchanged. After fabricating the photonic crystal structure as shown in Figure 1(e,f), we remove the Al_2O_3 and SiO_2 layers and perform the APM defect etch and an RCA clean before completing the front-end and back-end processing as described for the baseline process. Figure 1b schematically shows the cell structure after back-end processing.

6.2. Etch Mask Definition

The thickness of the electron (e)-beam (JKLesker AXXIS) coated alumina (AlO_x target) was determined by ellipsometry (Woolam, VASE). Masks of 40–50 nm were investigated for optimisation of the laser ablation and plasma etch protocols. The refractive index $n + i\kappa \approx 1.595 + i0.011$ of alumina at 515 nm wavelength was determined by ellipsometry.

The standard objective-lens focusing was used for 515 and 343 nm fs-pulses to produce Gaussian intensity distribution at the focus. Also an axicon was used to form Bessel-beam-like intensity profile for 515 nm fs-laser pulses of 170 and 230 fs duration (Carbide and Pharos lasers, Light Conversion). Details on pulse duration, focusing, and exposure conditions are presented where it applies. The axicon used in this study was fs-laser inscribed inside silica glass for $\lambda = 515$ nm wavelength. The form-birefringence of nano-gratings was used to engineer refractive index of concentric grating for the required phase retardance. The cone angle of the flat axicon corresponded to 178°. A $f =$ 400 mm lens with $20^{\times} NA = 0.4$ objective lens was used to scale

down the Bessel beam using an optical 4F-relay scheme. The final cone angle on the sample was $\gamma = 18.46°$, the diameter of $d^B_{min} = 1.24\ \mu$m at the first minimum or 0.88 µm at $1/e^2$-intensity level. The length of the non-diffracting Bessel beam zone was ~400 µm. Laser ablation was carried out at pulse fluence several time larger than 0.2 J/cm^2, which is the ablation threshold of Si at the used conditions.[26]

6.3. Bessel Beam Patterning of Alumina Mask

The Direct Laser Write (DLW) by 515 nm/167 fs laser pulses with Bessel beam focusing was carried out on POLO^2-IBC Si solar cells (7 cells per 4-inch wafer). The second harmonics of laser emission at the direct absorption of Si served two functions: 1) there was no long-pulse pedestal for the ultra-short fs-pulse and energy deposition was purely by 515 nm pulse and 2) the deposition of energy through an optically transparent mask was the most shallow. The shallow energy deposition into skin depth $1/\alpha$ facilitates the removal of laser-affected volume during plasma etching through the ablated hole, here α is the absorption coefficient. The transparent alumina 41 ± 1 nm mask was deposited by electron (e)-beam coating (JK Lesker, AXXIS) on the face-side of the POLO^2-IBC Si solar cells. Single pulse per ablation site was used to write 2.2 × 2.2 cm^2 masks of $\Lambda = 3.1$ µm period square lattice pattern at $v_{sc} = 7.5$ cm/s scan speed and laser repetition rate was $f = 0.6$ MHz. The axial extension of the laser pulse $ct_p \approx 50$ µm and the depth-of-focus $DoF \sim 400$ µm at the used focusing conditions. Pulse energy was $E_p = 44 \pm 1$ nJ.

Supporting Information

Supporting Information is available from the Wiley Online Library or from the author.

Acknowledgements

The authors thank G. Glowatzki, R. Zieseniß (both Leibniz Univerität Hannover), S. Spätlich and R. Winter (both ISFH) for sample processing. This work was funded by the German Federal Ministry for Economic Affairs and Climate Protection within the research project "27Plus6" (grant FKZ 003EE1056A) and by the Australian Government within the project ARC DP190103284 "Photonic crystals: the key to breaking the silicon-solar cell efficiency barrier." This work was partially funded by the federal state of Lower Saxony and the European Union's Horizon Europe research and innovation program under grant agreement No. 101146684. This work was performed in part at the Melbourne Centre for Nanofabrication (MCN) in the Victorian Node of the Australian National Fabrication Facility (ANFF). The authors thank Workshop-of-Photonics (WOP) Ltd., Lithuania for the patent license and technology transfer project by which the industrial fs-laser fabrication setup was acquired for Nanolab, Swinburne.

Conflict of Interest

The authors declare no conflict of interest.

Data Availability Statement

The data that support the findings of this study are available from the corresponding author upon reasonable request.

Keywords

Bessel beam, femtosecond laser ablation, light trapping, periodically anchored mask, photonic crystal textures, silicon solar cells

Received: July 14, 2025
Revised: September 8, 2025
Published online: November 6, 2025

[1] R. Peibst, M. Rienäcker, Y. Larionova, N. Folchert, F. Haase, C. Hollemann, S. Wolter, J. Krügener, J. Bayer, M. Dzinnik, R. Haug, R. Brendel, **2022**, *238*, 111560.
[2] pv magazine, Longi claims world's highest efficiency for silicon solar cells, **2025**, https://pv-magazine-usa.com/2025/04/14/longi-claims-worlds-highest-efficiency-for-silicon-solar-cells-2/?utm_source=USA+%7C+Newsletter&utm_campaign=db5116b046-dailynl_us&utm_medium=email&utm_term=0_80e0d17bb8-db5116b046-160597244&ct=t(dailynl_us).
[3] S. Bhattacharya, S. John, *Phys. Rev. Appl.* **2018**, *9*, 044009.
[4] M.-L. Hsieh, A. Kaiser, S. Bhattacharya, S. John, S.-Y. Lin, *Sci. Rep.* **2020**, *10*, 11857.
[5] S. Bhattacharya, S. John, *APL Photonics* **2020**, *5*, 020902.
[6] S. Bhattacharya, S. John, *Opt. Express* **2024**, *32*, 29795.
[7] M. S. Branham, W.-C. Hsu, S. Yerci, J. Loomis, S. V. Boriskina, B. R. Hoard, S. E. Han, G. Chen, *Adv. Mater.* **2015**, *27*, 2182.
[8] A. Gaucher, A. Cattoni, C. Dupuis, W. Chen, R. Cariou, M. Foldyna, L. Lalouat, E. Drouard, C. Seassal, P. Roca i Cabarrocas, et al., *Nano Lett.* **2016**, *16*, 5358.
[9] M. A. Green, Z. Zhou, *Opt. Express* **2025**, *33*, 37499.
[10] S. Bhattacharya, S. John, *Opt. Express* **2025**, *33*, 37503.
[11] J. Maksimovic, J. Hu, S. Ng, T. Katkus, G. Seniutinas, T. Pinedo Rivera, M. Stuiber, Y. Nishijima, S. John, S. Juodkazis, *Opto-Electron Adv* **2022**, *5*, 210086.
[12] K. Kumar, K. K. C. Lee, P. R. Herman, J. Nogami, N. P. Kherani, *Appl. Phys. Lett.* **2012**, *101*, 222106.
[13] B. Yang, M. Lee, *Opt. Laser Technol.* **2014**, *63*, 120.
[14] B. Voisiat, S. Indrišiūnas, R. Suzanovičienė, I. Šimkienė, G. Račiukaitis, in *Laser Processing and Fabrication for Solar, Displays, and Optoelectronic Devices III*, Proc. of SPIE, (Ed.: E. W. Reutzel), vol. *9180*, Bellingham, Washington, **2014**, p. 918009.
[15] T. Katkus, S. H. Ng, H. Mu, N. H. A. Le, D. Stonytė, Z. Khajehsaeidimahabadi, G. Seniutinas, J. Baltrukonis, O. Ulčinas, M. Mikutis, V. Sabonis, Y. Nishijima, M. Rienäcker, U. Römer, J. Krügener, R. Peibst, S. John, S. Juodkazis, *Adv. Eng. Mater.* **2024**, 2400711.
[16] B. Kafle, J. Seiffe, M. Hofmann, L. Clochard, E. Duffy, J. Rentsch, *Phys. Status Solidi A* **2015**, *212*, 307.
[17] F. Haase, C. Hollemann, S. Schäfer, A. Merkle, M. Rienäcker, J. Krügener, R. Brendel, R. Peibst, *Sol. Energy Mater. Sol. Cells* **2018**, *186*, 184.
[18] M. Rienäcker, Y. Larionova, J. Krügener, S. Wolter, R. Brendel, R. Peibst, *EPJ Photovolt.* **2021**, *12*, 6.
[19] D. E. Kane, R. M. Swanson, in *Proceedings of the 18th IEEE Photovoltaic Specialists Conference (PVSC)*, **1985**, pp. 578–583.
[20] W. Wu, P. K. McLarty, *J. Vac. Sci. Technol., A* **1995**, *13*, 67.
[21] M. Rienäcker, Ph.D. Thesis, Leibniz Universität Hannover, **2022**.
[22] S. J. Fonash, *J. Electrochem. Soc.* **1990**, *137*, 3885.
[23] G. Oehrlein, *Mater. Sci. Eng., B* **1989**, *4*, 441.
[24] G. Kumaravelua, M. M. Alkaisia, D. W. Macdonaldb, J. Zhaoc, B. Rongd, A. Bittare, *Engineering, Materials Science, Physics* **2005**.
[25] M. Kim, K. H. Min, S. Park, H. Song, J. I. Lee, K. T. Jeong, J. Park, M. Kang, *Curr. Appl. Phys.* **2020**, *20*, 519.
[26] J. Bonse, S. Baudach, J. Krüger, W. Kautek, M. Lentzner, *Appl. Phys. A* **2002**, *74*, 19.